Implanted hair-follicle-associated pluripotent (HAP) stem cells differentiating to keratinocytes, macrophages and endothelial cells accelerated cutaneous wound closure and suppressed scar formation in a mouse model

Koya Obara（✉ obarakoya@gmail.com ）

  Kitasato University School of Medicine: Kitasato Daigaku Igakubu https://orcid.org/0000-0002-5235-3161

Kyoumi Shirai

  Kitasato University School of Medicine: Kitasato Daigaku Igakubu

Yuko Hamada

  Kitasato University School of Medicine: Kitasato Daigaku Igakubu

Nobuko Arakawa

  Kitasato University School of Medicine: Kitasato Daigaku Igakubu

Ayami Hasegawa

  Kitasato University School of Medicine: Kitasato Daigaku Igakubu

Nanao Takaoka

  Kitasato University School of Medicine: Kitasato Daigaku Igakubu

Ryoichi Aki

  Kitasato University School of Medicine: Kitasato Daigaku Igakubu

Robert M. Hoffman

  Anti cancer inc.

Yasuyuki Amoh

  Kitasato University School of Medicine: Kitasato Daigaku Igakubu

Abstract

Background

Patients frequently experience physical, mental, and even financial distress because of acute or chronic wounds to the skin. In severe situations, the skin scars can be quite noticeable, cause persistent discomfort, restrict joint motion, or be mentally taxing. Hair-follicle-associated pluripotent (HAP) stem cells were discovered by our laboratory, in the bulge area of hair follicle; and can differentiate to neurons, glia, beating cardiomyocytes, keratinocyte and nascent vessel. In the present study, we determined if HAP stem cells can accelerate cutaneous wound healing in a mouse model.

Methods

HAP stem cells which were grown from the upper part of vibrissa follicle and formed a sheet in culture were implanted to dorsal wounds in a mouse model. After HAP-stem-cell-sheet-implantation, progression of wound closure with time was evaluated. After wound closure, scar morphology, infiltration of dermal inflammatory cell such as macrophage and fibrocyte and dermal fibrosis were observed histologically. mRNA of TGF-β1, type I collagen alpha 2 (COL1A2) and type III collagen alpha 1 (COL3A1) expression levels in the wound were measured by quantitative real-time PCR (RT-PCR) to assess dermal inflammation and fibrosis.

Results

HAP stem cells formed sheet which differentiated to keratinocytes, macrophages and endothelial cells in culture. After HAP-stem-cell-sheet-implantation to the dorsal wound in the mice model, it accelerated the wound closure, increased capillary-vessel-formation and suppressed macrophage and fibrocyte infiltration and collagen deposition in the dermis compared with non-implanted control mice. Also, mRNA of TGF-β1, COL1A2 and COL3A1 expression levels in the wound were decreased in the HAP-stem-cell-implanted mice compared with non-implantation control mice.

Conclusions

Implantation of HAP stem cells differentiated to keratinocytes, macrophages and endothelial cells accelerated wound closure and suppressed scar formation in a mouse model, indicating clinical potential of scar-free wound healing.

Introduction

The skin is often injured by acute or chronic wounds, such as trauma, burns, diabetic ulcers and venous stasis ulcers, causing physical and emotional distress in patients and an even economic distress. The main goals of wound management are proper wound care, including "wound bed preparation" and "moist wound healing" is important for complete wound healing and ointment treatments are used to ameliorate the wound bed commonly [1, 2]. However, due to local and systemic variables, the wound healing is

susceptible to dysregulation, which can result in healing failure and the development of chronicity. [3]. When wounds transitioned to intractable and chronic, they often do not heal or heal very slowly. When the skin scars changed quite prominent, such as keloids and hypertrophic scars also after wound healing, it can cause chronic pain, or limited joint movement, or psychological burden in severe cases [4]. Thus, there is a need for treatment methods that allow early closure of cutaneous wounds and inhibit scar formation. Recent studies have shown that stem cell therapy has enormous promise for regenerating skin tissue [5]. When transplanted into a wound, stem cells promote cell mobilization, immunomodulation, extracellular matrix remodeling, and angiogenesis, either directly or in a paracrine manner, by secreting cytokines and growth factors [6–8].

Hair-follicle-associated pluripotent (HAP) stem cells, discovered by our laboratory [9], reside in the bulge area of hair follicle [9, 10], express nestin and have multilineage differentiation capacity to produce neurons, glia, smooth muscle cells, melanocytes, keratinocytes, nascent blood vessels, adipocytes and beating cardiac muscle cells [11–15]. In the present study, we demonstrated that HAP-stem-cell-sheet-implantation for cutaneous wound in a mouse model can affect structural and functional recovery. The potential clinical advantages of HAP stem cells for wound therapy are discussed.

Materials And Methods

Animals

Transgenic C57BL/6J-EGFPmice (GFP mice) were acquired from the Research Institute for Microbial Diseases (Osaka University, Osaka, Japan) [16]. C57BL/6J mice and BALB/cAJcl-nu/nu mice (nude mice) were acquired from CLEA Japan (Tokyo, Japan). The experimental animals were kept in an animal housing system maintained at 24 ± 1°C, relative humidity of 50–60%, and 14 hours of light 10 hours of dark intervals. All procedures involving animals complied with the guidelines of the US National Institutes of Health and were approved by the Animal Experimentation and Ethics Committees of the Kitasato University School of Medicine (No. 2021-024). All efforts were made to minimize animal suffering and reduce the number of animals used. The method of euthanasia at the end of the experiment was cervical dislocation.

Isolation, culture, and sheet formation from HAP stem cells.

Vibrissa follicles were resected from green fluorescent protein (GFP) transgenic or non-GFP C57BL/6J mice as described previously [11]. To obtain the vibrissa follicles from mice, the animals were anesthetized with a combination anesthetic of 0.75 mg/kg medetomidine, 4.0 mg/kg midazolam and 5.0 mg/kg butorphanol [17]. The upper lip, containing the vibrissa pad, was extracted and its inside surface exposed. Binocular microscopy was used to dissect intact vibrissa follicles. The vibrissae were plucked from the vibrissa pad by pulling gently with a fine forceps. The upper part of the vibrissa follicles was separated as described previously [18]. The upper parts of the isolated vibrissa follicles were fixed to the adhesive cell culture dishes (Corning, NY, USA) with Matrigel® (Coring) and cultured in ciKIC iPS basal

medium (KANTO CHEMICAL, Tokyo, Japan) containing ciKIC iPS medium Supplement Set (KANTO CHEMICAL) for four weeks. Four weeks after culture, the growing GFP or non-GFP HAP stem cells formed sheet on the dishes.

Flow cytometry analysis.

Flow cytometry analysis performed previously reported [12, 14]. The growing cells were detached and incubated with anti-mouse CD34 RAM34 rat monoclonal antibody (1:200, eBioscience, CA, USA) and incubated with biotinylated anti-rat immunoglobulins (1:1,000, DAKO, CA, USA), then incubated with Brilliant Violet 421 streptavidin (1:500, BioLegend, CA, USA). Anti CD68 mouse monoclonal antibody (1:200, DAKO), anti Actin Smooth Muscle Ab-1 (α-SMA) mouse monoclonal antibody (1:200, Lab Vision, CA, USA), and keratin15 (K15) LHK15 mouse monoclonal antibody (1:200, Lab Vision), and then incubated with the secondary antibodies used were goat anti-mouse IgG H&L phycoerythrin (1:500, Abcam, Cambridge, UK) The cells were identified by FACS Verse (BD Bioscience, CA, USA). Data were analyzed by FACS suite™ software (BD Bioscience). FACS analysis was repeated in triplicate.

Implantation of HAP-stem-cell-sheet to cutaneous wounds in mouse model

A 10-mm round full-thickness excisional wounds was created in center of the dorsal of nude mice or C57BL/6J mice under anesthesia. Hydrocolloid dressing (DuoDERM, Convatec, Berkshire, UK) cut into Donut-shaped were fixed to the wound edges using 6−0 nylon sutures to prevent outflow of implanted cells. HAP-stem-cell-sheets were detached from the tissue culture dishes by gently rubbing from the sheet margin with a cell scraper (AS ONE, Osaka, Japan). The HAP-stem-cell-sheet containing approximately $6×10^5$ cells in 20 μL of PBS were applied to the dorsal wounds. A transparent, semi-occlusive adhesive dressing (Tegaderm, 3M, MN, USA) was then applied over the wounds for protection. The hydrocolloid dressing and semi-occlusive adhesive dressing was removed 2 days after implantation. The wounds were digitally photographed regularly after HAP stem cell implantation, and the wound size was measured through planimetrically using ImageJ software as previously [19].

Histological analysis.

At 21 days post-HAP-stem-cell implantation, the whole wound on the back of the mouse was removed after mouse sacrifice by cervical dislocation. Sections were made perpendicular to both the wound surface and the anterior−posterior axis. Raw specimens from both sides of the nude mouse wound were directly observed with fluorescence microscopy (Stereo Microscope SZX16, Olympus, Tokyo, Japan). The mouse wound tissue was the formalin-fixed, and paraffin-embedded-blocks (FFPB) were made. FFPB sections were stained using protocols for hematoxylin and eosin (H&E) and Masson's trichrome. The thickness of the wound in C57BL/6J mouse was determined considering the epidermis and the thin: thick ratio of epithelial thickness in H&E histological sections. The thickness of the dermis determined in Masson's trichrome histological sections as previously described [19, 20]. To determine the thickness of the epidermal layer or dermal layer, 3 high power fields (HPF) in one section per a mouse were randomly

selected, measured and averaged. In the thin: thick ratio of epithelial thickness, 1 HPF in one section per a mouse was randomly selected and measured. Quantitative analysis of dermal collagen in Masson's trichrome histological sections was performed using ImageJ software as previously described [21]. In the analysis of dermal collagen, 1 HPF in one section per mouse was randomly selected and quantified. All indices were analyzed using ImageJ software (version 1.52; National Institutes of Health, USA). The threshold values were maintained at a constant level for all analyses.

After immunofluorescence staining, the wound was observed by fluorescence microscopy (LSM 710 microscope, Carl Zeiss, Oberkochen, Germany). FFPB sections in nude mice were incubated with anti-CD34 rat monoclonal antibody (1:5000, eBioscience), anti-CD68 mouse monoclonal antibody (1:50, Dako) and anti-GFP rabbit monoclonal antibody (1:1000, Novus Biologicals, CO, USA). FFPB sections in C57BL/6J mice were incubated with anti-CD34 rat monoclonal antibody and ant-α-SMA mouse monoclonal antibody (1:200, Lab Vision). The anti-body-treated section then was incubated with goat anti-rat IgG conjugated with Alexa Fluor 568® (1:400, Molecular Probes, OR, USA), goat anti-rabbit IgG conjugated with Alexa Flour 488® (1:400, Molecular Probes) or goat anti-mouse IgG conjugated with Alexa Flour 568® (1:400, Molecular Probes) and 4',6-diamino-2-phenylindole, dihydrochloride (DAPI) (Molecular Probes). For immunostaining, FFPB sections from C57BL/6J mice on slides were incubated with anti-CD68 mouse monoclonal antibody, anti-transforming growth factor (TGF)-β1 mouse monoclonal antibody (1:100, Santa Cruz, TX, USA) and anti-inducible nitric oxide synthase (iNOS) rabbit monoclonal antibody (1:200, Biogenesis, CO, USA), and then were treated with Dako ChemMate Envision kit/HRP (Dako Japan, Tokyo, Japan). The sections were developed with 3,3'-diaminobenzidine tetrachloride (DAB) (Dako) and then incubated with Mayer's hematoxylin solution. DAB developed sections were observed by microscopy (BX 51 microscope, Olympus, Tokyo, Japan). Immunostaining for CD68, TGFβ1 and iNOS was then performed, in the wound and control. For analyzed immunofluorescence staining and immunostaining of immunolabeled cells, 3 HPF in one section per a mouse were randomly selected, quantified and averaged. All indices were analyzed using ImageJ software. The threshold values were maintained at a constant level for all analyses.

Quantitative Real-Time polymerase chain reaction (RT-PCR)

Total RNA was extracted from FFPB sections using the RNeasy Plus Mini Kit (Qiagen, Hilden, Germany), and cDNA was synthesized with QuantiTect® Reverse Transcription Kit (Qiagen) according to the manufacturer's instructions. cDNA was pre-amplified with Prelude PreAmp Master Mix (TAKARA, Shiga, Japan) and pooling primers. GAPDH was used to normalize gene expressions. Quantitative RT-PCR was performed using the Power SYBR® Green PCR Master mix (Applied Biosystems, MA, USA) on a CFX96 Real-Time PCR Detection System (Bio-Rad, CA, USA) and analyzed by the Delta Delta Ct method. Primer sequences were as follows: TGF-β1 (forward, GAGCCCGAAGCGGACTACTA; reverse, CCCGAATGTCTGACGTATTGAAG), type I collagen alpha 2 (COL1A2) (forward, GGTGAGCCTGGTCAAACGG; reverse, ACTGTGTCCTTTCACGCCTTT), type III collagen alpha 1 (COL3A1) (forward, CTGTAACATGGAAACTGGGGAAA; reverse, CCATAGCTGAACTGAAAACCACC), GAPDH (forward, AGGTCGGTGTGAACGGATTTG; reverse, TGTAGACCATGTAGTTGAGGTCA).

Statistical analysis.

All experimental data are expressed as the mean ± standard error. Data of the differences between groups with all histological analysis were analyzed with the unpaired Student's *t* test or Welch's *t* test according to the results of the *F* test. Two-way ANOVA followed by the Bonferroni post hoc test was used to examine the differences between groups in measurement of the back ulcer in C57BL/6J mice. A probability value of $P \leq 0.05$, $P \leq 0.01$, $P \leq 0.001$ and $P \leq 0.0001$ is considered significant.

Results

Differentiation of HAP-stem-cell-sheets

The upper parts of vibrissa follicles were cultured for 28 days. Under microscopy, polygonal shaped cells with spines were observed proliferated forming several layers around the vibrissa follicles in the culture dish. The cells that spread around vibrissa follicle were HAP stem cells that proliferating from the bulge area. The cultured HAP stem cells formed sheets (Fig. 1a). The HAP-stem-cell sheet was strong and could be gripped with a fine tweezer. HAP-stem-cell sheet obtained were analyzed by flow cytometry to verify its cell types. Flow cytometric analysis of HAP-stem-cell sheet showed high expression of K15 and low expression of α-SMA, CD34 and CD68 (Fig. 1b).

HAP-stem-cell-sheet-implantation accelerated cutaneous wound closure and suppressed scar formation in C57BL/6J mice

The HAP-stem-cell-sheet-implanted mice were observed in the wound healing area on between days 2 to 7 and days 11 to 14, as compared with non-implanted control mice (P = 0.0099 at day 2; P = 0.0243 at day 3; P = 0.0147 at day 4; P = 0.0226 at day 5; P = 0.0222 at day 6; P = 0.0098 at day 7; P = 0.014 at day 11; P = 0.0115 at day 12; P = 0.0037 at day 13; P = 0.0163 at day 14) (Fig. 1c). Two days after HAP-stem-cell-implantation for the dorsal wound, the surface of wounded area was covered with a translucent sheet structure. The sheet covered the surface of wounded areas until 8–12 days after implantation, but it fell off the wound thereafter.

The morphology of wound for each group was evaluated histologically (Fig. 2a). The HAP-stem-cell-sheet-implanted mice showed a significantly thinner in the epidermis than non-implanted control mice (P = 0.0024) (Fig. 2b). When the thickness of the epidermis of wound relative to the nearby normal skin was quantified (thin: thick ratio), the thin: thick ratio of the epidermis in the HAP-stem-cell-sheet-implanted mice approached normal mouse skin, as compared with the wound in the non-implanted control mice (P = 0.0033) (Fig. 2c). Masson's trichrome staining revealed dense collagenous tissue formation in the non-implanted control mice. In contrast a more complex collagen structure with collagen bundles distributed in multiple levels was observed in the dermis of the HAP-stem-cell-sheet-implanted mice (Fig. 2d). The

HAP-stem-cell-sheet-implanted mice showed significantly thinner in the dermis than non-implanted control mice (P = 0.0012) (Fig. 2e). The HAP-stem-cell-sheet-implanted mice showed significantly less collagen deposition than non-implanted control mice (P = 0.0019). (Fig. 2f).

Implanted HAP-stem-cell-sheet differentiated to endothelial cells and macrophage in the cutaneous wound in nude mice

Nude mice were used in this experiment in order to readily visualize the GFP-expressing HAP stem cells in the wound. At 21 days post-HAP-stem-cell-sheet-implantation, the repaired dorsal wound in nude mice was directly observed with a stereomicroscopy which showed that GFP-expressing HAP stem cells joined the wound. GFP-expressing HAP stem cell formed large and small aggregates and extensively branched fine network in the dermis (Fig. 3a). Immunofluorescence staining showed that the implanted GFP-expressing HAP stem cells differentiated to endothelial cells that exhibit tube structure and express CD34 and macrophages that exhibit oval shaped and express CD68 in the wound. No GFP-expressing HAP stem cells in the epidermis were observed. (Fig. 3b).

HAP-stem-cell-sheet-implantation promoted angiogenesis and suppressed fibrocyte infiltration in the cutaneous wound in C57BL/6J mice

Immunofluorescence staining, newly formed capillary vessels in the wound were identified as tube structure co-stained for CD34 and α-SMA staining and originally mature vessels in the wound were identified as tube structure stained for α-SMA staining, respectively (Fig. 4a). The number of newly formed capillary vessels increased significantly along during healing process in HAP-stem-cell-sheet-implanted mice as compared with the non-implanted control mice (P = 0.0022) (Fig. 4b). CD34-positive, α-SMA-negative, and spindle-shaped cells were observed in the dermis, identified as fibrocytes (Fig. 4a). The HAP-stem-cell-sheet-implanted mice had significantly fewer fibrocytes in the wound than non-implanted control mice (P = 6.58×10^{-5}) (Fig. 4c).

HAP-stem-cell-sheet-implantation suppressed macrophage infiltration and inhibited the expression of TGF-β1 and iNOS in the cutaneous wound in C57BL/6J mice

The HAP-stem-cell-sheet implanted mice had significantly fewer CD68 positive macrophages in the wound than non-implanted control mice in immunostaining (P = 9.19×10^{-4}) (Fig. 5a, b). HAP-stem-cell-sheet-implanted mice had significantly less signals of TGF-β1 (P = 0.0030) and iNOS (P = 0.0048) in the dermis than non-implanted control mice (Fig. 5a, c, d).

HAP-stem-cell-sheet-implantation decreases the expression of TGF-β1, COL1A2 and COL3A1 in the wound of C57BL/6J mice.

In the wound of mice implanted with HAP-stem-cell-sheets, the mRNA expression of TGFβ-1 ($P = 0.0170$), COL1A2 ($P = 0.0462$) and COL3A1 ($P = 0.0251$) was significantly decreased compared with non-implanted control mice (Fig. 6a–c).

Discussion

The primary component of the skin barrier is the epidermis, which is made up of a multilayered epithelium with appendages. It's crucial to restore the skin barrier function and quickly rebuild the epidermis after wounding. The wound healing process can be divided into three phases. Numerous circulating cell types, including neutrophils and macrophages, are transported to the site of injury during the inflammatory phase. In contrast, keratinocytes, fibroblasts, fibrocytes, and endothelial cells move and multiply during the proliferative phase, leading in epithelization and granulation. To finish tissue repair during the remodeling phase, excessive collagen deposition in the wound is disassembled by a proteolytic enzyme [22, 23].

In the present study, the dorsal wound of mice implanted with HAP-stem-cell-sheets accelerated closing compared to non-implanted control mice. Two days after HAP-stem-cell-sheet-implantation in the dorsal wound, the surface of wounded area was covered with a sheet structure. The sheet covered the surface of wounded areas until 8–12 days after implantation, but it fell off wound after that. And in nude mice implanted with GFP-expressing HAP stem cell, these cells were not observed in epidermis of wound 21 days after implantation. It is possible that epidermal turnover was not established in the HAP-stem-cell-sheets implanted to the wound. However, keratinocyte have been reported to produce keratin, keratinocyte-derived granulocyte-macrophage colony stimulating factor and Ccl2, and play an important role in re-epithelialization [24–27]. Thus, keratinocytes are crucial for the cutaneous wound healing, and the keratinocytes differentiated from HAP stem cells are assumed to have promoted the wound closure.

The macrophage is one of the major types of infiltrating leukocytes after injury [28–30]. Macrophages are involved in all phases of tissue repair, performing essential functions in inflammation and debris removal in the early stages of wounding and transitioning to functions that support healing during the regenerative phase [31–35]. In the present study, HAP-stem-cell-sheets implanted to the cutaneous wound differentiated to macrophages which may have affected early wound healing.

On the other hand, it has also been demonstrated that macrophages regulate the development of scars and that reducing their numbers during the initial stages of repair limits the development of scars [36]. Additionally, macrophages produce TGF- and iNOS, two cytokines that have been demonstrated to prevent excessive scarring and wound fibrosis [38–40]. In the present study, the wound implanted with HAP-stem-cell-sheets was suppressed macrophage infiltration and expression of TGF-β1 and iNOS. As a result, HAP-stem-cell-sheet-implantation is possibility inhibited wound fibrosis and scar formation.

R Recent investigations have also revealed that the fibrocyte cell type has a role in the healing of wounds. Hematopoietic cells that express CD34 and type I collagen are known as fibrocytes, and they have a spindle-shaped appearance [41]. Fibrocyte is implicated in pathological fibrosis, such as skin, aorta, lung,

and kidney fibrosis, in addition to physiological wound healing [42]. In the present study, fibrocytes infiltrated the wound significantly more in the non-implanted control mice than HAP-stem-cell-sheet-implanted mice. HAP-stem-cell-sheet-implantation may have suppressed fibrocyte infiltration, wound fibrosis and subsequent scar formation.

In the present study, HAP-stem-cell-sheets implanted into wound differentiated to endothelial cells and promoted angiogenesis in the wound. We recently reported that new vessels grow from the HAP stem cells, and number of vessels increased when the local recipient skin is wounded [43]. To provide oxygen and nutrients to the wound cells, angiogenesis is essential for wound healing [44]. Numerous studies have shown that increased angiogenesis can effectively enhance wound healing [45, 46]. Lack of angiogenesis during the inflammatory phase of wound healing may cause transition to chronic wound [47]. HAP-stem-cell-sheet-implantation accelerated wound closure by differentiating to endothelial cells and promoting angiogenesis in the wound.

Various stem cell therapy has been reported potentially to promote cutaneous wound healing and reduce post-wound fibrosis. However, Due to their immunogenicity, tumorigenicity, and ethical issues, embryonic stem cells (ESCs) are challenging to employ in therapeutic settings [48]. Induced pluripotent stem cells (iPSCs) have the potential to develop tumors like teratoma, which is a problem [49]. Mesenchymal stem cells (MSCs) can be isolated from bone marrow, cord blood, peripheral blood and adipose tissue [50–52]. The extraction of MSCs is time consuming and the number of cells that can be harvested is confined. In contrast to other stem cell therapy, HAP stem cells, used in the present study, are readily accessible from everyone, and can be used autologously without immune-suppression, do not form tumors, and can be cryopreserved without loss of pluripotency, allowing individualized banking [11, 53, 54].

Conclusion

In summary, closure of wounds with keratinocytes differentiated from HAP stem cells was accelerated. Differentiation of the implanted HAP stem cells to macrophages in the wound and the regulation of macrophage infiltration decreased inflammation in the wound. Suppressed of fibrocyte infiltration by implanted HAP stem cells and wound fibrosis thereby decreasing scar formation. Differentiation of HAP stem cell to new endothelial cells promoted of angiogenesis in the wound. Therefore, HAP stem cells used in the present study have important potential to be an effective future clinical strategy for accelerating wound healing.

Abbreviations

HAP: Hair-follicle-associated pluripotent

SMA: Actin smooth muscle

K15: Keratin15

FFPB: Formalin-fixed, and paraffin-embedded-blocks

HPF: High power fields

DAPI: 4',6-diamino-2-phenylindole, dihydrochloride

TGF: Transforming growth factor

iNOS: Inducible nitric oxide synthase

DAPI: 3,3'-diaminobenzidine tetrachloride

RT-PCR: Real-Time polymerase chain reaction

COL1A2: Type I collagen alpha 2

COL3A1: Type III   collagen alpha 1

ESCs: Embryonic stem cells

iPSCs: Induced pluripotent stem cells

MSCs: Mesenchymal stem cells

Declarations

Availability of data materials

The datasets generated and analyzed during the current study are available from the first author (Koya Obara) on reasonable request.

Author information

Authors and Affiliations

Department of Dermatology, Kitasato University School of Medicine, Sagamihara, Kanagawa, 252-0374, Japan

Koya Obara, Kyoumi Shirai, Yuko Hamada, Nobuko Arakawa, Ayami Hasegawa, Nanako Takaoka, Ryoichi Aki & Yasuyuki Amoh

AntiCancer, Inc., San Diego, CA, 92111, USA

Robert M. Hoffman

Department of Surgery, University of California San Diego, San Diego, CA, 92103, USA

Robert M. Hoffman

Contributions

KO designed and performed the experiment and analyzed the results. YH and NA carried out the experiments and data analysis. KO wrote and YH, RMH and YA revised this manuscript. All authors read and approved the final draft of the manuscript.

Corresponding author

Correspondence to Robert M. Hoffman or Yasuyuki Amoh

Ethics declarations

Ethics approval and consent to participate

All procedures involving animals complied with the guidelines of the US National Institutes of Health and were approved by the Animal Experimentation and Ethics Committees of the Kitasato University School of Medicine (No. 2021-024).

Consent for publication

Not applicable in this section.

Competing interests

All of the authors declare that they have no competing interests.

References

1. Harries RL, Bosanquet DC, Harding KG. Wound bed preparation: TIME for an update. Int Wound J. 2016;13 Suppl 3(Suppl 3):8–14.
2. Winter GD. Formation of the scab and the rate of epithelization of superficial wounds in the skin of the young domestic pig. Nature. 1962;193:293–4.
3. Sheehan P, Jones P, Caselli A, Giurini JM, Veves A. Percent change in wound area of diabetic foot ulcers over a 4-week period is a robust predictor of complete healing in a 12-week prospective trial.

Diabetes Care. 2003;26(6):1879–82.

4. Spiekman M, van Dongen JA, Willemsen JC, Hoppe DL, van der Lei B, Harmsen MC. The power of fat and its adipose-derived stromal cells: emerging concepts for fibrotic scar treatment. J Tissue Eng Regen Med. 2017;11(11):3220–35.

5. Kanji S, Das H. Advances of stem cell therapeu tics in cutaneous wound healing and regeneration. Mediators Inflamm. 2017;2017:5217967.

6. Isakson M, de Blacam C, Whelan D, McArdle A, Clover AJP. Mesenchymal stem cells and cutaneous wound healing: current evidence and future potential. Stem Cells Int. 2015;2015:831095.

7. Cao Y, Gang X, Sun C, Wang G. Mesenchymal stem cells improve healing of diabetic foot ulcer. J Diabetes Res. 2017;2017:9328347.

8. Mizukami H, Yagihashi S. Exploring a new therapy for diabetic polyneuropathy - the application of stem cell transplantation. Front Endocrinol. 2014;5:45.

9. Li L, Mignone J, Yang M, Matic M, Penman S, Enikolopov G, Hoffman RM. Nestin expression in hair follicle sheath progenitor cells. Proc Natl Acad Sci U S A. 2003;100(17):9958–61

10. Uchugonova A, Duong J, Zhang N, König K, Hoffman RM. The bulge area is the origin of nestin-expressing pluripotent stem cells of the hair follicle. J Cell Biochem. 2011;112(8):2046–50.

11. Amoh Y, Li L, Katsuoka K, Penman S, Hoffman RM. Multipotent nestin-positive, keratin-negative hair-follicle bulge stem cells can form neurons. Proc Natl Acad Sci U S A. 2005;102(15):5530–4.

12. Yashiro M, Mii S, Aki R, Hamada Y, Arakawa N, Kawahara K, Hoffman RM, Amoh Y. From hair to heart: nestin expressing hair follicle associated pluripotent (HAP) stem cells differentiate to beating cardiac muscle cells. Cell Cycle. 1015;14(14):2362–6.

13. Amoh Y, Mii S, Aki R, Hamada Y, Kawahara K, Hoffman RM, Katsuoka K. Multipotent nestin-expressing stem cells capable of forming neurons are located in the upper, middle, and lower part of the vibrissa hair follicle. Cell Cycle. 2012;11(18):3513–7.

14. Yamazaki A, Yashiro M, Mii S, Aki R, Hamada Y, Arakawa N, Kawahara K, Hoffman RM, Amoh Y. Isoproterenol directs hair follicle-associated pluripotent (HAP) stem cells to differentiate in vitro to cardiac muscle cells which can be induced to form beating heart muscle tissue sheets. Cell Cycle. 2016;15(5):760–5.

15. Amoh Y, Li L, Yang M, Moossa AR, Katsuoka K, Penman S, Hoffman RM. Nascent blood vessels in the skin arise from nestin-expressing hair-follicle cells. Proc Natl Acad Sci U S A. 2004;101(36):13291–5.

16. Okabe M, Ikawa M, Kominami K, Nakanishi T, Nishimune Y. 'Green mice' as a source of ubiquitous green cells. FEBS Letters. 1997;407(3):313–9.

17. Kawai S, Takagi Y, Kaneko S, Kurosawa T. Effect of three types of mixed anesthetic agents alternate to ketamine in mice. Experimental Animals. 2011;60(5):481–7.

18. Amoh Y, Mii S, Aki R, Hamada Y, Kawahara K, Hoffman RM, Katsuoka K. Multipotent nestin-expressing stem cells capable of forming neurons are located in the upper, middle, and lower part of

the vibrissa hair follicle. Cell Cycle. 2012;11(18):3513–7.

19. Yu J, Wang MY, Tai HC, Cheng NC. Cell sheet composed of adipose-derived stem cells demonstrates enhanced skin wound healing with reduced scar formation. Acta Biomater. 2018;77:191-200.

20. Li P, Liu P, Xiong RP, Chen XY, Zhao Y, Lu WP, Liu X, Ning YL, Yang N, Zhou YG. Ski, a modulator of wound healing and scar formation in the rat skin and rabbit ear. J Pathol. 2011;223(5):659–71.

21. Motta MM, Stelini RF, Calderoni DR, Gilioli R, Damiani GV, César CL, Kharmandayan P. Effects of the lower energy and pulse stacking in carbon dioxide laser skin treatment: an objective analysis using second harmonic generation. Acta Cir Bras. 2021;36(3):e360304.

22. Martin P. Wound healing-aiming for perfect skin regeneration. Science. 1997;276(5309):75–81.

23. Suga H, Rennert RC, Rodrigues M, Sorkin M, Glotzbach JP, Januszyk M, Fujiwara T, Longaker MT, Gurtner GC.Tracking the elusive fibrocyte: identification and characterization of collagen-producing hematopoietic lineage cells during murine wound healing. Stem Cells. 2014;32(5):1347–60.

24. Sahin U, Türeci Ö. Personalized vaccines for cancer immunotherapy. Science. 2018;359(6382):1355–60.

25. Martln-Fontecha A, Sebastiani S, Höpken UE, Uguccioni M, Lipp M, Lanzavecchia A, Sallusto F. Regulation of dendritic cell migration to the draining lymph node: impact on T lymphocyte traffic and priming. J Exp Med. 2003;198(4):615–21.

26. Mann A, Breuhahn K, Schirmacher P, Blessing M. Keratinocyte-derived granulocyte-macrophage colony stimulating factor accelerates wound healing: Stimulation of keratinocyte proliferation, granulation tissue formation, and vascularization. J Invest Dermatol. 2001;117(6):1382–90.

27. Han Y, Villarreal-Ponce A, Gutierrez G Jr, Nguyen Q, Sun P, Wu T, Sui B, Berx G, Brabletz T, Kessenbrock K, et al. Keratinocyte-Macrophage Crosstalk by the Nrf2/Ccl2/EGF Signaling Axis Orchestrates Tissue Repair. Cell Rep. 2020;33(8):108417.

28. Eming SA, Krieg T, Davidson JM. Inflammation in wound repair: molecular and cellular mechanisms. J Invest Dermatol. 2007;127(3):514–25.

29. Guo S, Dipietro LA. Factors affecting wound healing. J Dent Res. 2010;89(3):219–29.

30. Werner S, Grose R. Regulation of wound healing by growth factors and cytokines. Physiol Rev. 2003;83(3):835–70.

31. Aurora AB, Olson EN. Immune modulation of stem cells and regeneration. Cell Stem Cell. 2014;15(1):14–25.

32. Wynn TA, Vannella KM. Macrophages in tissue repair, regeneration, and fibrosis. Immunity. 2016;44(3):450–462.

33. Lucas T, Waisman A, Ranjan R, Roes J, Krieg T, Müller W, Roers A, Eming SA. Differential roles of macrophages in diverse phases of skin repair. J Immunol. 2010;184(7):3964–77.

34. Lechner AJ, Driver IH, Lee J, Conroy CM, Nagle A, Locksley RM, Rock JR. Recruited monocytes and Type 2 immunity promote lung regeneration following pneumonectomy. Cell Stem Cell. 2017;21(1):120–134.e7.

35. Knipper JA, Willenborg S, Brinckmann J, Bloch W, Maaß T, Wagener R, Krieg T, Sutherland T, Munitz A, Rothenberg ME, et al. Interleukin-4 Receptor α Signaling in Myeloid Cells Controls Collagen Fibril Assembly in Skin Repair. Immunity. 2015;43(4):803−816.

36. Feng Y, Sun ZL, Liu SY, Wu JJ, Zhao BH, Lv GZ, Du Y, Yu S, Yang ML, Yuan FL, et al. Direct and indirect roles of macrophages in hypertrophic scar formation. Front Physiol. 2019;10:1101.

37. James R, Hesketh MA, Benally TR, Johnson SS, Tanner LR, Means SV. Macrophage Phenotypes Regulate Scar Formation and Chronic Wound Healing. Int J Mol Sci. 2017;18(7):1545.

38. Xu X, Zheng L, Yuan Q, Zhen G, Crane JL, Zhou X, Cao X. Transforming growth factor-β in stem cells and tissue homeostasis. Bone Res. 2018;6:2.

39. Zhang T, Wang XF, Wang ZC, Lou D, Fang QQ, Hu YY, Zhao WY, Zhang LY, Wu LH, Tan WQ. Current potential therapeutic strategies targeting the TGF-β/Smad signaling pathway to attenuate keloid and hypertrophic scar formation. Biomed Pharmacother. 2020;129:110287.

40. Cash JL, Bass MD, Campbell J, Barnes M, Kubes P, Martin P. Resolution mediator chemerin15 reprograms the wound microenvironment to promote repair and reduce scarring. Curr Biol. 2014;24(12):1406−14.

41. Bucala R, Spiegel LA, Chesney J, Hogan M, Cerami A. Circulating fibrocytes define a new leukocyte subpopulation that mediates tissue repair. Mol Med. 1994;1(1):71−81.

42. Bellini A, Mattoli S. The role of the fibrocyte, a bone marrow-derived mesenchymal progenitor, in reactive and reparative fibroses. Lab Invest. 2007;87(9):858−70.

43. Amoh Y, Li L, Yang M, Moossa AR, Katsuoka K, Penman S, Hoffman RM. Nascent blood vessels in the skin arise from nestin-expressing hair-follicle cells. Proc Natl Acad Sci U S A. 2004;101(36):13291−5.

44. Zhu Z, Liu Y, Xue Y, Cheng X, Zhao W, Wang J, He R, Wan Q, Pei X. Tazarotene Released from Aligned Electrospun Membrane Facilitates Cutaneous Wound Healing by Promoting Angiogenesis. ACS Appl Mater Interfaces. 2019;11(39):36141−53.

45. Su CH, Li WP, Tsao LC, Wang LC, Hsu YP, Wang WJ, Liao MC, Lee CL, Yeh CS. Enhancing Microcirculation on Multitriggering Manner Facilitates Angiogenesis and Collagen Deposition on Wound Healing by Photoreleased NO from Hemin-Derivatized Colloids. ACS Nano. 2019;13(4):4290−301.

46. Wang P, Huang S, Hu Z, Yang W, Lan Y, Zhu J, Hancharou A, Guo R, Tang B. In situ formed anti-inflammatory hydrogel loading plasmid DNA encoding VEGF for burn wound healing. Acta Biomater. 2019;100:191−201.

47. Bauer SM, Bauer RJ, Velazquez OC. Angiogenesis, vasculogenesis, and induction of healing in chronic wounds. Vasc Endovasc Surg. 2005;39(4):293−306.

48. Coraux C, Hilmi C, Rouleau M, Spadafora A, Hinnrasky J, Ortonne JP, Dani C, Aberdam D. Reconstituted skin from murine embryonic stem cells. Curr Biol. 2003;13(10):849−53.

49. Okita K, Ichisaka T, Yamanaka S. Generation of germline-competent induced pluripotent stem cells. Nature. 2007;448(7151):313−317.

50. Coalson E, Bishop E, Liu W, Feng Y, Spezia M, Liu B, Shen Y, Wu D, Du S, Li AJ, et al. Stem cell therapy for chronic skin wounds in the era of personalized medicine: from bench to bedside. Genes Dis. 2019;6(4):342–358.

51. Yu JR, Navarro J, Coburn JC, Mahadik B, Molnar J, Holmes JH 4th, Nam AJ, Fisher JP. Current and future perspectives on skin tissue engineering: key features of biomedical research, translational assessment, and clinical application. Adv Healthc Mater. 2019;8(5):e1801471.

52. Nourian Dehkordi A, Mirahmadi Babaheydari F, Chehelgerdi M, Raeisi Dehkordi S. Skin tissue engineering: wound healing based on stem-cell-based therapeutic strategies. Stem Cell Res Ther. 2019;10(1):111.

53. Obara K, Tohgi N, Mii S, Hamada Y, Arakawa N, Aki R, Singh SR, Hoffman RM, Amoh Y. Hair-follicle-associated pluripotent stem cells derived from cryopreserved intact human hair follicles sustain multilineage differentiation potential. Sci Rep. 2019;9(1):9326.

54. Kajiura S, Mii S, Aki R, Hamada Y, Arakawa N, Kawahara K, Li L, Katsuoka K, Hoffman RM, Amoh Y. Cryopreservation of the hair follicle maintains pluripotency of nestin-expressing stem cells. Tissue Eng Part C Methods. 2015;21(8):825–31.
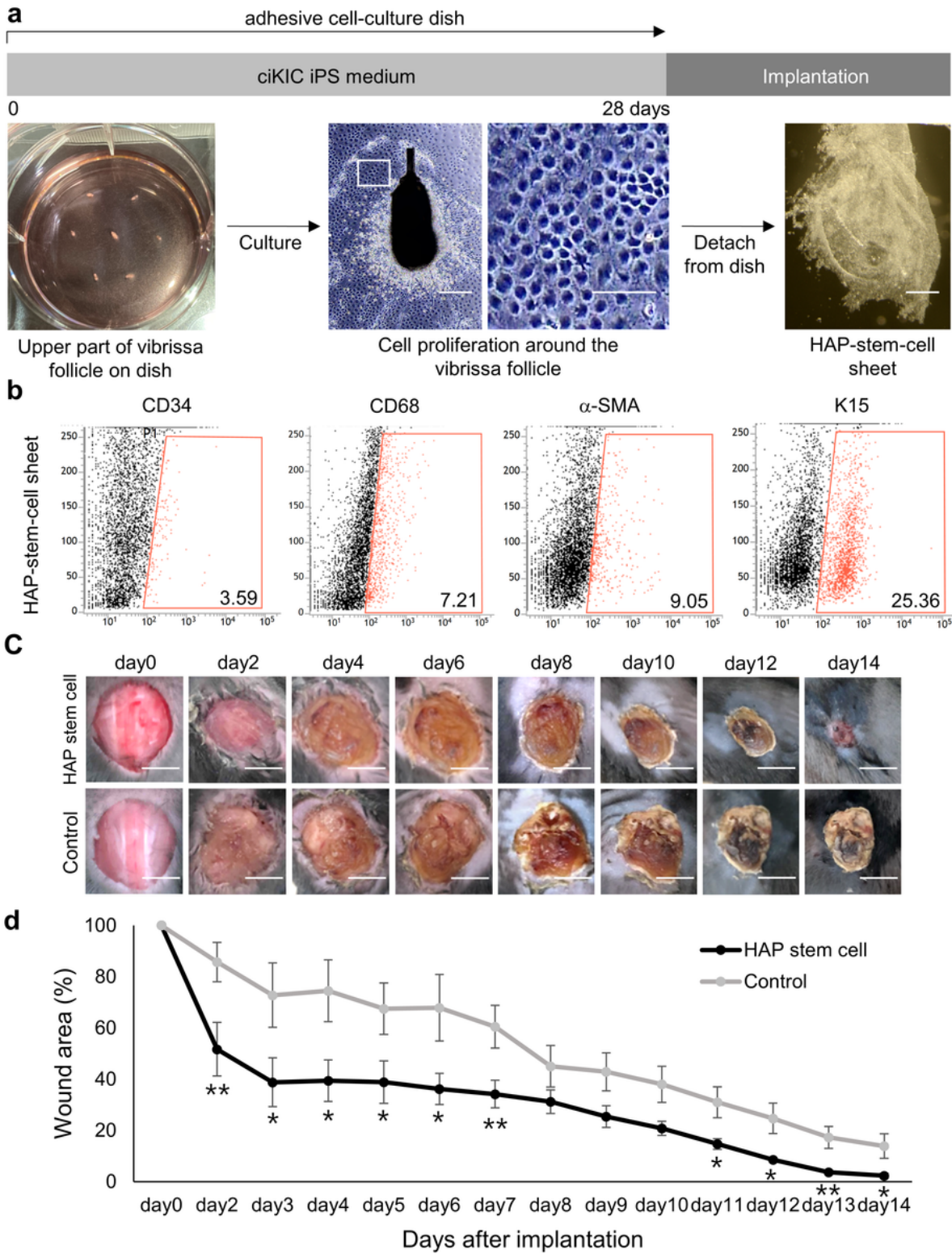
Figures

Figure 1

Characterization of HAP stem-cell-sheets and their effect on cutaneous wound in C57BL/6J mice after implantation. **a** Schematic of HAP-stem-cell-sheet formation process. Scale bars = 500μm (low power field), 100μm (high power field). **b** Flow cytometric analysis of CD34-positive, CD68-positive, α-SMA-positive, and K15-positive cells in HAP-stem-cell-sheets. c Photographs of representative dorsal wounds in C57BL/6J mice implanted with HAP-stem-cell-sheets (upper row) or without implantation (lower row)

post-wounding. Scale bars = 5mm. d Time course of wound closure for HAP-stem-cell-sheet implantation and non-implanted control mice (n = 8, each group). *$P < 0.05$, **$P < 0.01$.
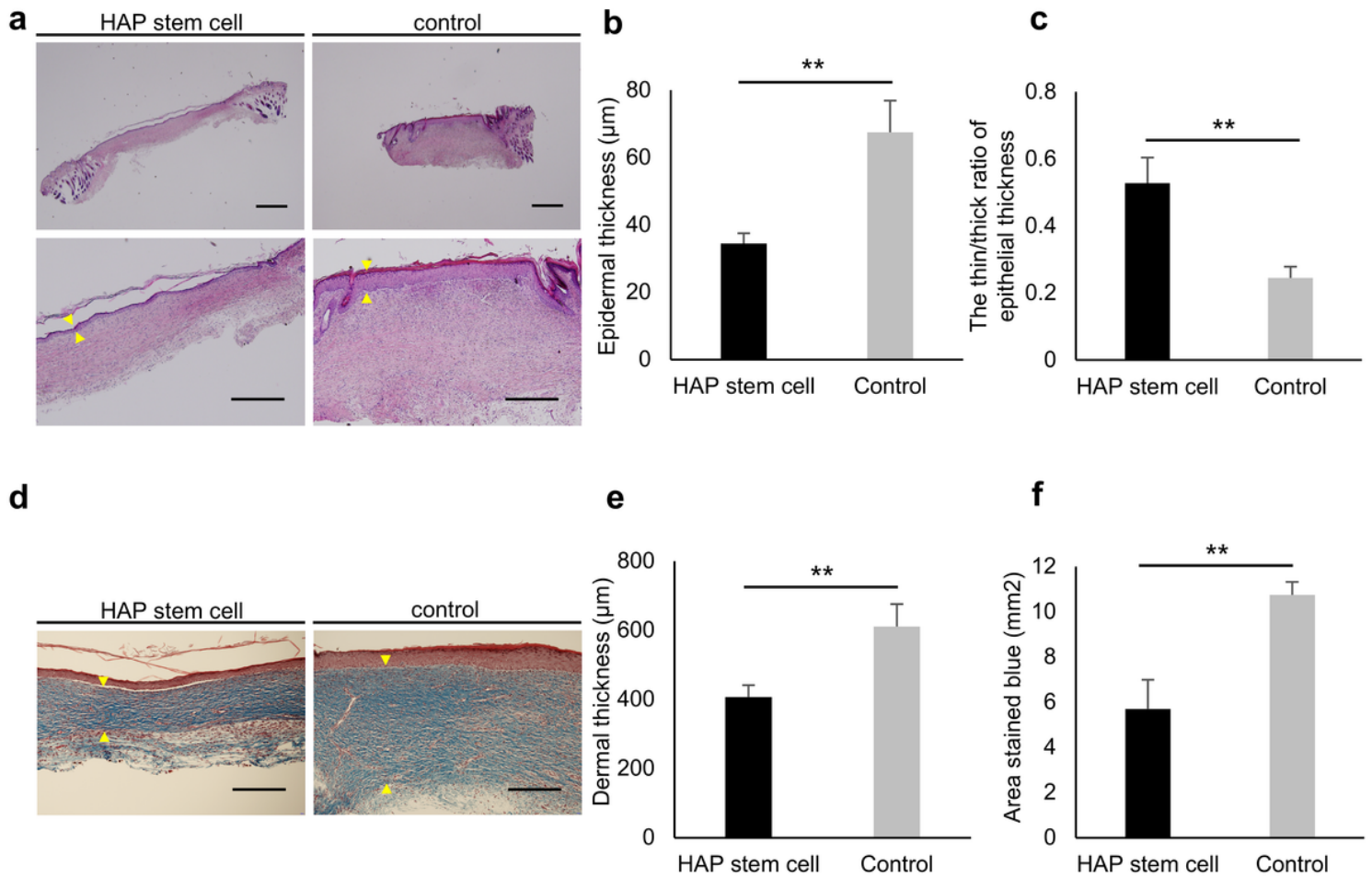
Figure 2

Characterization of wound healing after HAP-stem-cell-sheet-implantation in C57BL/6J mice. **a** Representative images of wound healing seen in H&E staining of tissue sections. Scale bars = 1mm (low power field), 500μm (high power field). Epidermal thickness (yellow arrow). **b** Quantitative analysis of epidermal thickness in H&E stained sections (n = 8, each group). **$P < 0.01$. **c** The thin: thick ratio of epithelial thickness in H&E stained sections (n = 6, each group). **$P < 0.01$. **d** Representative images of wound healing seen in Masson's trichrome staining of tissue sections. Scale bars = 500μm. Dermal thickness (yellow arrow). **e** Quantitative analysis of dermal thickness in Masson's trichrome stained sections (n = 10. **$P < 0.01$. **f** Quantitative analysis of collagen deposition in Masson's trichrome stained sections (n = 7, each group). **$P < 0.01$
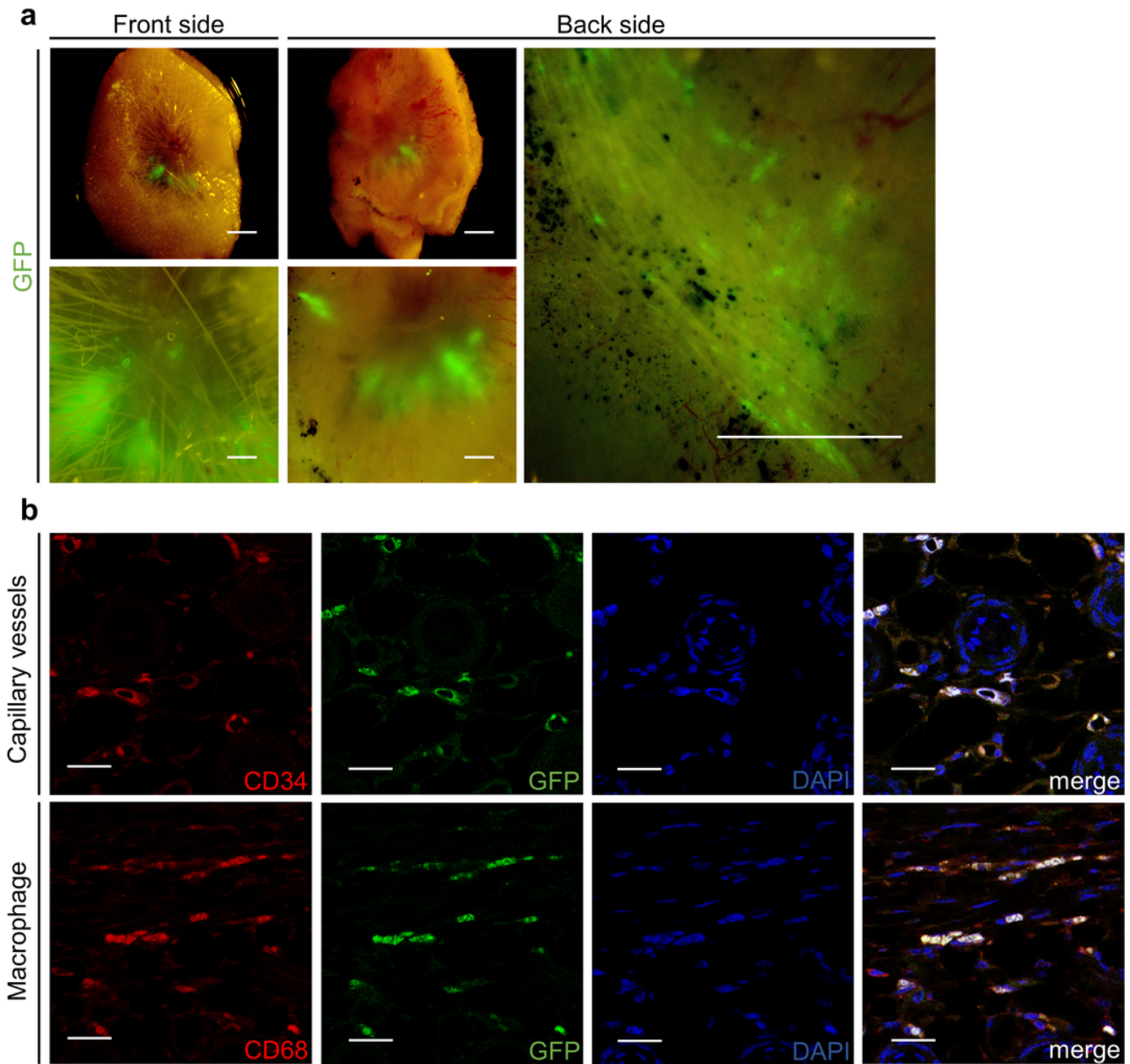
Figure 3

Engraftment and differentiation of HAP-stem-cell-sheets after implantation to cutaneous wounds in nude mice. **a** Front and back of raw specimen of the wound directly observed with fluorescence microscopy. Scale bars = 2mm (low power field), 500μm (high power field). **b** Immunofluorescence staining analysis of expressing CD34 (upper row) or CD68 (lower row) (red) and GFP (green), together with DAPI staining (blue). Scale bars = 50μm.
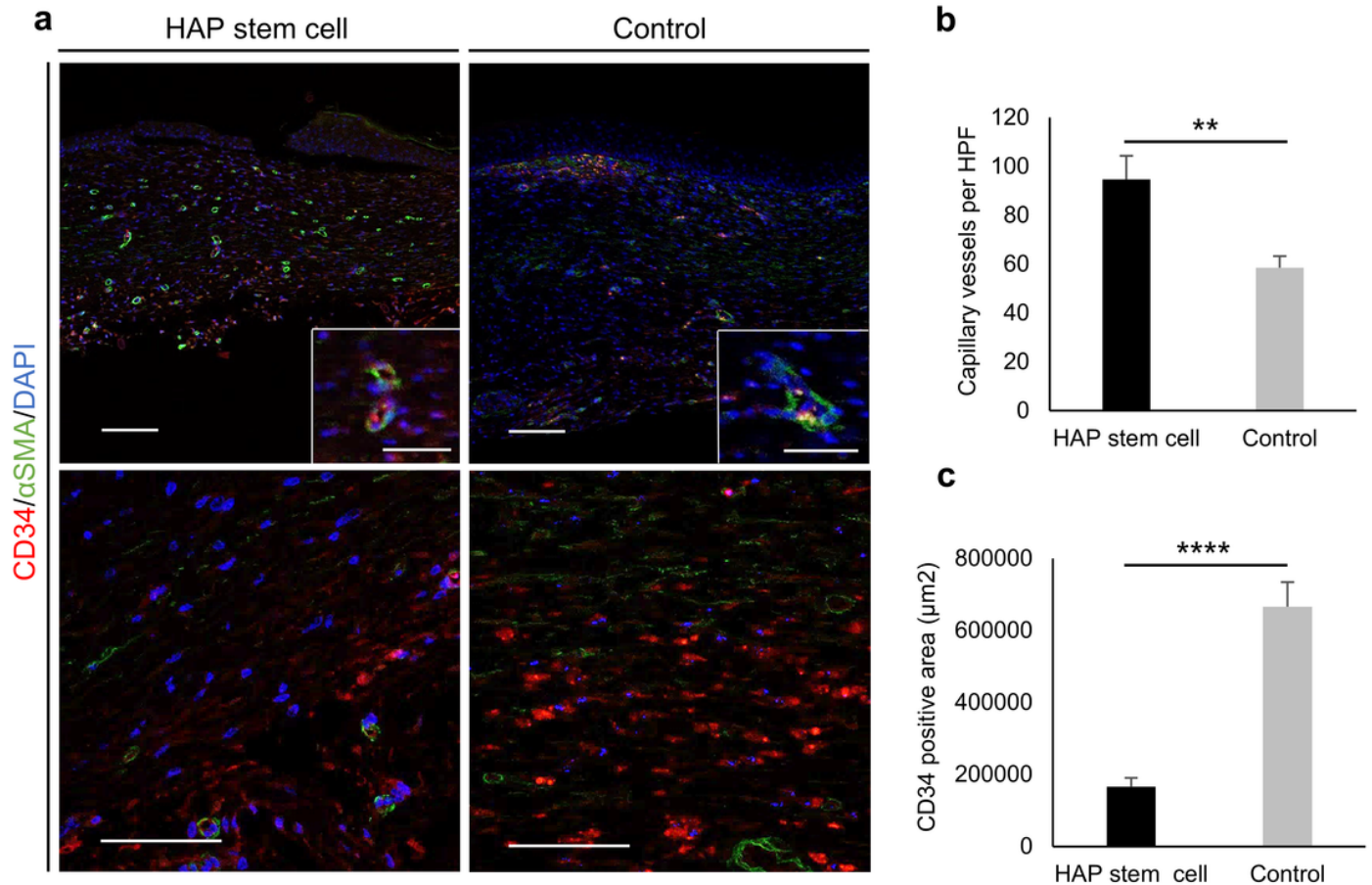
Figure 4

Capillary vessels and fibrocyte in the wound of C57BL/6J mice after HAP-stem-cell-sheet-implantation. **a** Representative images of CD34 (red) and α-SMA (green), together with DAPI staining (blue) seen with immunofluorescence staining. Scale bars = 200μm (low power field), 50μm (high power field). **b** Quantitative analysis of tube structures expressing CD34 and α-SMA seen with immunofluorescence staining (n = 8, each group). **$P < 0.01$. **c** Quantitative analysis of spindle shaped cells expressing CD34 with immunofluorescence staining (n = 5, each group). ****$P < 0.0001$.
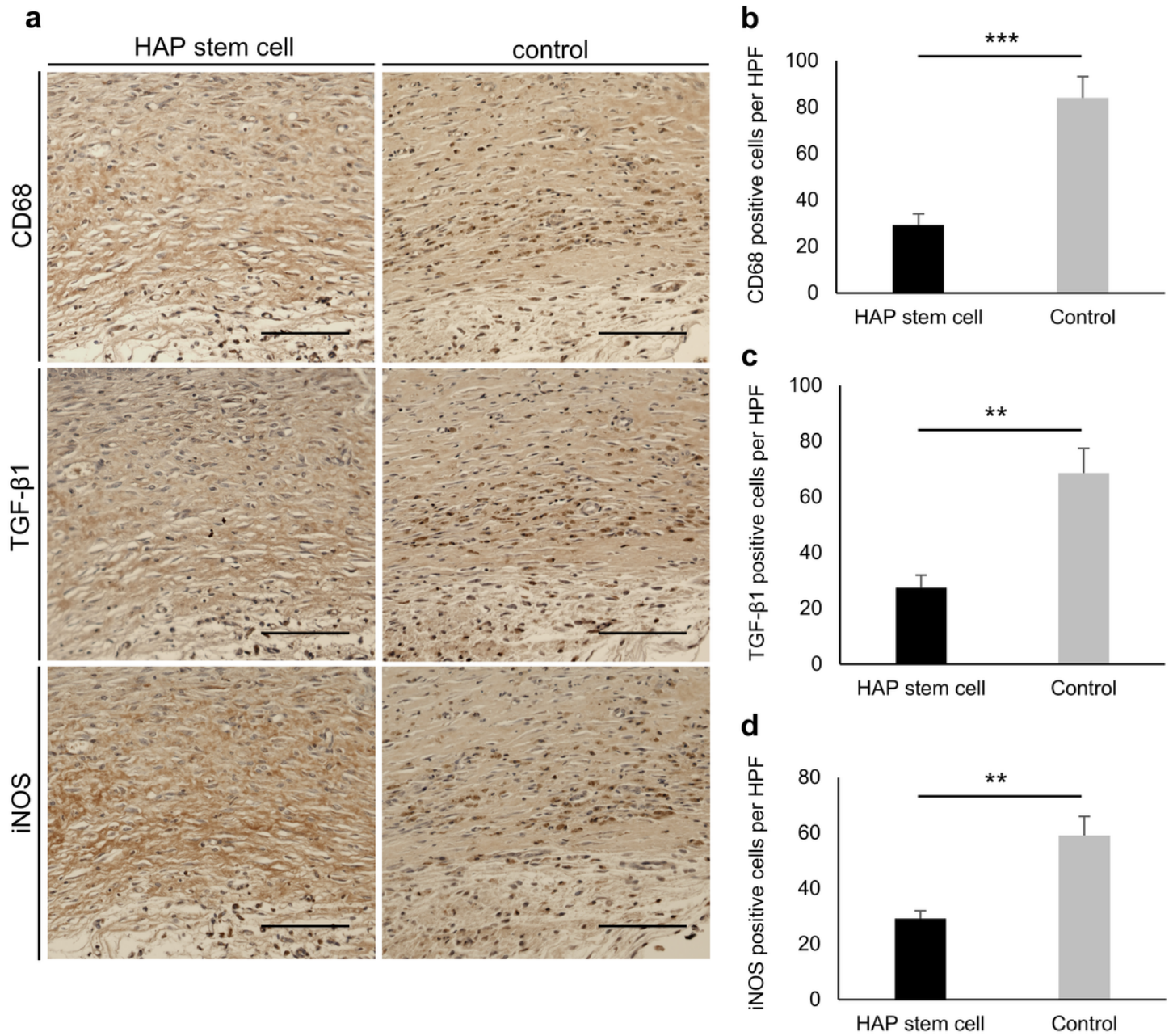
Figure 5

Effect of HAP-stem-cell-sheet implantation on dermal macrophage in the wound of C57BL/6J mice. a Representative images of CD68, TGF-β1 and iNOS seen with immunostaining. Scale bars = 200μm. b Quantitative analysis of immunostaining of CD68. (n = 5, each group) ***$P < 0.001$. c Quantitative analysis of immunostaining of TGF-β1. (n = 5, each group) **$P < 0.01$. d Quantitative analysis of immunostaining of iNOS. (n = 5, each group) **$P < 0.01$.
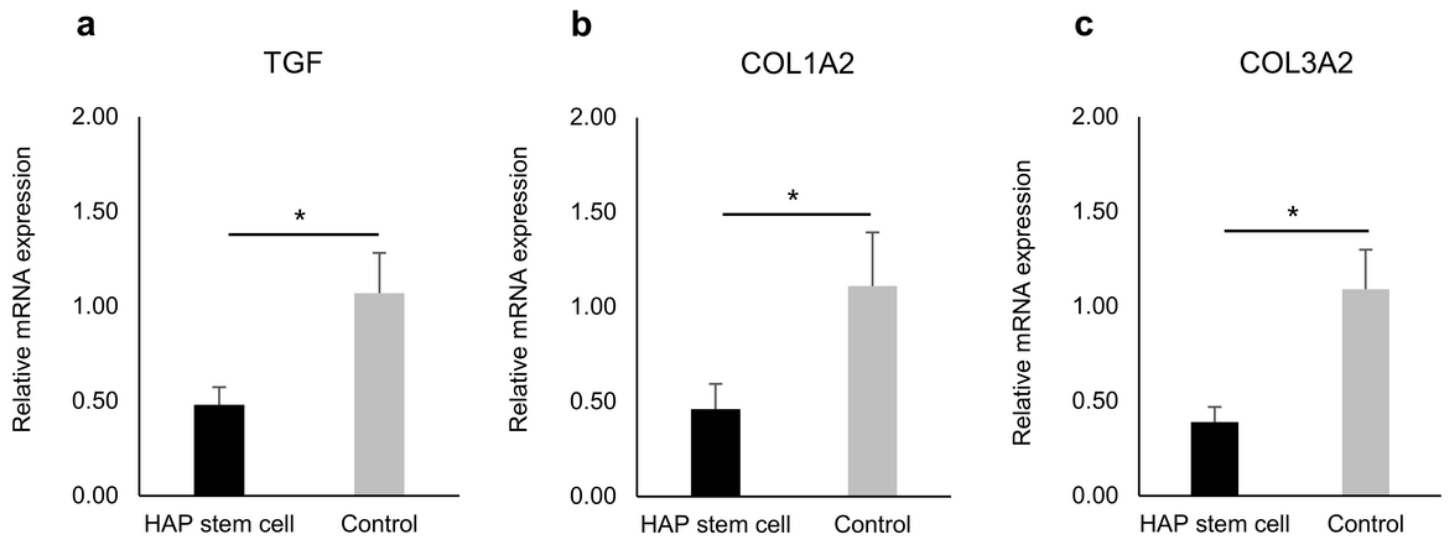
Figure 6

Relative mRNA expression levels of TGF-β1 (HAP-stem-cell-implanted mice: n = 5; non-implanted control mice: n = 7), COL1A2 (HAP-stem-cell-implanted mice: n = 5; non-implanted control mice: n = 7) and COL3A1 (HAP-stem-cell-implanted mice: n = 5; non-implanted control mice: n = 7) measured by quantitative RT-PCR in the wound of C57BL/6J mice. *$P < 0.05$.